Chemistry–A European Journal
Full Paper
doi.org/10.1002/chem.202101859
Chemistry Europe
European Chemical Societies Publishing

Stability of Ag^{III} towards Halides in Organosilver(III) Complexes

Daniel Joven-Sancho,[a] Miguel Baya,[a] Larry R. Falvello,[b] Antonio Martín,[a] Jesús Orduna,[b] and Babil Menjón*[a]

Dedicated to the Memory of Prof. Dr. Víctor Riera

Abstract: The involvement of silver in two-electron Ag^{I}/Ag^{III} processes is currently emerging. However, the range of stability of the required and uncommon Ag^{III} species is virtually unknown. Here, the stability of Ag^{III} towards the whole set of halide ligands in the organosilver(III) complex frame $[(CF_3)_3AgX]^-$ (X=F, Cl, Br, I, At) is theoretically analyzed. The results obtained depend on a single factor: the nature of X. Even the softest and least electronegative halides (I and At) are found to form reasonably stable Ag^{III}–X bonds. Our estimates were confirmed by experiment. The whole series of nonradiative halide complexes $[PPh_4][(CF_3)_3AgX]$ (X=F, Cl, Br, I) has been experimentally prepared and all its constituents have been isolated in pure form. The pseudohalides $[PPh_4][(CF_3)_3AgCN]$ and $[PPh_4][(CF_3)_3Ag(N_3)]$ have also been isolated, the latter being the first silver(III) azido complex. Except for the iodo compound, all the crystal and molecular structures have been established by single-crystal X-ray diffraction methods. The decomposition paths of the $[(CF_3)_3AgX]^-$ entities at the unimolecular level have been examined in the gas phase by multistage mass spectrometry (MS^n). The experimental detection of the two series of mixed complexes $[CF_3AgX]^-$ and $[FAgX]^-$ arising from the corresponding parent species $[(CF_3)_3AgX]^-$ demonstrate that the Ag–X bond is particularly robust. Our experimental observations are rationalized with the aid of theoretical methods. Smooth variation with the electronegativity of X is also observed in the thermolyses of bulk samples. The thermal stability in the solid state gradually decreases from X=F (145 °C, dec.) to X=I (78 °C, dec.) The experimentally established compatibility of Ag^{III} with the heaviest halides is of particular relevance to silver-mediated or silver-catalyzed processes.

Introduction

The involvement of silver in two-electron redox processes was only recently demonstrated.[1,2] This new paradigm opens a wealth of possibilities for a metal, which has been traditionally confined to a limited role as a one-electron reagent. As a result of these new findings, novel Ag^{III} species belonging to the select class of high-valent organometallic derivatives[3] are now considered as feasible reaction intermediates. A key step in this new reactivity pattern for silver is the oxidative addition of a halocarbon, RX, to the Ag^{I} centre to afford the oxidized R–[Ag^{III}]–X entity. The success of this crucial step depends on the ease with which the R–X bond is cleaved and on the stability of the final product. In general, the R–X bond is more easily broken on going down the halogen Group: F < Cl < Br < I. For this reason, the heavier R–Br and R–I molecules are preferentially used over the lighter R–F and R–Cl ones in this kind of process.[1a] However, the reducing ability of the halide ions follows exactly the same trend, an unfortunate coincidence that might compromise the stability and even the credibility of any tentative R–[Ag^{III}]–I intermediate. In this context, it is worth noting that the transient species $[Me_2RAgI]^-$ presumably formed upon oxidative addition of R–I to the homoleptic $[Me_2Ag]^-$ derivative could not be detected either even using the most advanced spectroscopic techniques.[4] In actual fact, there is a lack of experimental evidence confirming the existence of these critical and elusive intermediates.

Oxidation state III is still rare for silver and the highest currently available for this metal.[5,6] The only known binary silver(III) halide is the fluoride AgF_3,[7] which is unstable and extremely reactive.[8] Complex fluorides include the paramagnetic material $Cs_2K[AgF_6]$[9] and a number of salts of the square-planar diamagnetic anion $[AgF_4]^-$ (Scheme 1).[10] In contrast, none of the heavier AgX_3 halides (X=Cl, Br, I) has ever been prepared. In fact, they were calculated to be unstable in the gas phase and better viewed as $XAg{\cdot}X_2$ adducts (Scheme 1).[11] In a recent study, Grochala et al. showed that the silver(II) chloride,

[a] D. Joven-Sancho, Dr. M. Baya, Dr. A. Martín, Dr. B. Menjón
Instituto de Síntesis Química y Catálisis Homogénea (iSQCH)
CSIC-Universidad de Zaragoza
C/ Pedro Cerbuna 12, 50009 Zaragoza (Spain)
E-mail: menjon@ctq.csic.es

[b] Prof. Dr. L. R. Falvello, Dr. J. Orduna
Instituto de Nanociencia y Materiales de Aragón (INMA)
CSIC-Universidad de Zaragoza
C/ Pedro Cerbuna 12, 50009 Zaragoza (Spain)

Supporting information for this article is available on the WWW under https://doi.org/10.1002/chem.202101859

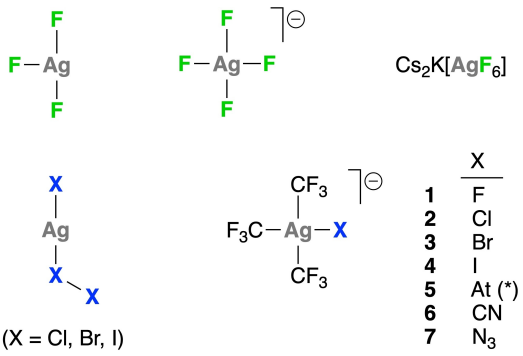

Scheme 1. Currently known silver(III) fluorides and other related halides (see text for details). Compounds **1**–**7** are studied in this work. Aside from the astato complex **5**, all other compounds were isolated and characterized.

$AgCl_2$, was metastable in the solid state with respect to $AgCl + {}^1/_2Cl_2$.[12] The heavier halides $AgBr_2$ and AgI_2 are known to be even less stable.[13] In the realm of organometallic chemistry, we recently found that the organosilver(III) fluoride $[PPh_4][(CF_3)_3AgF]$ shows an ideal combination of thermal stability and chemical reactivity, as was briefly communicated.[14] The heavier organosilver(III) halides $[(CF_3)_3AgX]^-$ (X=Cl, Br, I) had been detected in solution by Eujen, Hoge and Brauer, but could not be isolated.[15] Although the isolation of the $[N(PPh_3)_2][(CF_3)_3AgX]$ (X=Cl, Br) salts was later claimed,[16] only fragmentary information and insufficient data were reported. Thus, little is known about the compatibility of Ag^{III} with the heavier halides.

Here, we provide a theoretical evaluation of the compatibility of Ag^{III} with every halogen, including the heaviest naturally occurring one: At. Furthermore, we first isolate compounds with Ag^{III}–Br and Ag^{III}–I bonds, thereby lending experimental support for the existence of related transient and intermediate species. An unprecedented silver(III) azido complex, $[PPh_4][(CF_3)_3Ag(N_3)]$, has also been obtained, isolated and characterized.

Results and Discussion

Synthetic procedures

Considering the existing precedents,[15,16] the solvento complex $(CF_3)_3Ag(NCMe)$ might be viewed as the most suitable synthon of the $(CF_3)_3Ag$ moiety. This widely sought complex is known to arise in different processes and under various conditions, yet in nonselective means. The most successful synthesis among them all involves treatment of $Li[(CF_3)_4Ag]$ with ICl in MeCN to eventually afford the desired product in only about 8% estimated yield.[16] Its isolation as a colorless oil is, however, intriguing, since the gold homologue $(CF_3)_3Au(NCMe)$ is known to be a white solid.[17] In the search for an alternative synthesis, it becomes apparent that, aside from the extremely reactive AgF_3 and $[AgF_4]^-$ species, there is a lack of suitable Ag^{III} precursors. A different synthetic strategy was therefore needed.

Thus, we turned to the homoleptic Ag^I complex $[CF_3AgCF_3]^-$ as a potential precursor. The most straightforward method would be the oxidative addition of CF_3I to the Ag^I homoleptic precursor $[CF_3AgCF_3]^-$. This method with optimal atom economy was successfully applied in gold chemistry. Thus, the photoinduced oxidative addition of CF_3I to the linear complex $[CF_3AuCF_3]^-$ cleanly afforded the square-planar gold(III) derivative $[(CF_3)_3AuI]^-$ and provided an efficient entry to the $(CF_3)_3Au$ moiety.[18] This procedure, however, failed when applied to the Ag^I precursor (Scheme 2). On the other hand, it has been recently reported that the non-fluorinated homologous species $[Me_2Ag]^-$ underwent oxidative addition of MeI at low temperature.[4] Although the primary product, $[Me_3AgI]^-$, could not be directly detected, its intermediacy was inferred from the nature of the final derivatives formed.

Access to the $(CF_3)_3Ag$ moiety was in general not easy because the formation of the homoleptic species $[(CF_3)_4Ag]^-$ is largely favored. It can be said that this symmetric, fully substituted compound acts as a thermodynamic sink in many of these processes. In fact, it was the main compound obtained by treatment of $[CF_3AgCF_3]^-$ with $PhI(OAc^F)_2$ and Me_3SiCF_3 in the presence of CsF (Scheme 2).[19] In this context, it is worth noting that the chloro complex $[(CF_3)_3AgCl]^-$ was first detected (^{19}F NMR) as an intermediate species in the synthesis of the mixed-valence salt $Ag[(CF_3)_4Ag]$ by Dukat and Naumann.[20] Isolation of the chloro complex proved difficult though. The material obtained by reacting DME solutions of $[PPh_4][(CF_3)_3AgCN]$ with AcCl was later reported to consist of $[PPh_4][(CF_3)_3AgCl]$ with around 90% purity content as estimated by spectroscopic methods.[15] In a subsequent work, the $[N(PPh_3)_2][(CF_3)_3AgCl]$ salt was purportedly isolated as a white solid in 33.7% yield by treating MeCN solutions of the aforementioned solvento complex $(CF_3)_3Ag(NCMe)$ with $[N(PPh_3)_2]Cl$ followed by column-chromatography purification. Unfortunately, no analytic data were provided and therefore, the purity of the obtained material is unknown.[16]

We have devised a more convenient method to obtain analytically pure samples of the salt $[PPh_4][(CF_3)_3AgCl]$ (**2**), which consisted of treating $[PPh_4][CF_3AgCF_3]$ with $PhICl_2$ in CH_2Cl_2 solution at −55 °C (Scheme 2). The procedure involved both metal oxidation and ligand exchange. Only $^2/_3$ of the total metal amount suffered oxidation from Ag^I to Ag^{III}, whereas the remaining $^1/_3$ portion acted as CF_3-transfer reagent. As a result,

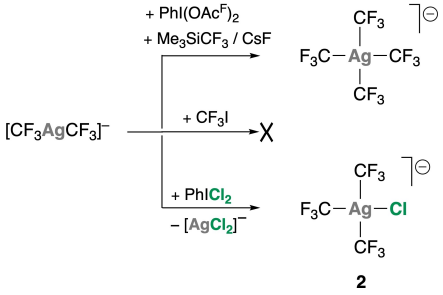

Scheme 2. Ag^I is successfully oxidized to Ag^{III} with the organoiodine(III) reagents $PhI(OAc^F)_2$ (see ref. [19]) and $PhICl_2$, but not with CF_3I.

the silver(I) halide complex $[PPh_4][AgCl_2]$ was formed along with the desired product. Fortunately, this inorganic byproduct was efficiently removed by taking advantage of its virtual insolubility in DME.[21] In this way, compound **2** was finally isolated as a pale-yellow solid in 75% yield with respect to the theoretical amount expected in the indicated process (Scheme 2).

With complex **2** in hand, we wanted to check whether the Ag^{III} ion belongs to class *a* or class *b* metals according to the Ahrland–Chatt–Davis classification,[22] which directly relates to the more general *hard* and *soft* classification.[23] To this aim, we treated complex **2** with alkali metal salts of the heavier halides (KBr, NaI) in CH_2Cl_2 solution at room temperature. Under these experimental conditions, substitution did actually occur and the heavier homologues $[(CF_3)_3AgBr]^-$ and $[(CF_3)_3AgI]^-$ were formed. The process, however, was not clean and the corresponding complexes could not be isolated in pure form, at least under the assayed conditions. Although of little synthetic use, the process sufficed to classify the Ag^{III} ion within the class *b* (soft) metals in analogy to the well-established behavior of Au^{III}.[24] The isolation of compounds $[PPh_4][(CF_3)_3AgBr]$ (**3**) and $[PPh_4][(CF_3)_3AgI]$ (**4**) required a different synthetic approach (see below).

According to the class *b* behavior of Ag^{III}, all previous attempts to prepare the lighter fluoro complex $[(CF_3)_3AgF]^-$ by halide exchange with fluoride were unsuccessful.[15] The reaction of the solvento complex $(CF_3)_3Ag(NCMe)$ with $[N(PPh_3)_2]F$, KF and HF also failed.[16] We have found, however, that the reaction of complex **2** with AgF in MeCN (Scheme 3) affords the fluoro-derivative $[PPh_4][(CF_3)_3AgF]$ (**1**), which is isolated as a white solid in 75% yield.[14] This is the first organosilver(III) fluoride compound to have been prepared or even detected. Our preliminary assays demonstrated that the terminal F-ligand in compound **1** is reactive, as it readily undergoes solvolysis with H_2O and with thiols RSH.[14] We took further advantage of the reactivity of this unique compound.

The fluoro complex **1** provides an efficient entry to the heavier halide homologues $[(CF_3)_3AgBr]^-$ and $[(CF_3)_3AgI]^-$, which had eluded isolation to date. It is worth noting that although Naumann et al. claimed the isolation of the bromo complex $[N(PPh_3)_2][(CF_3)_3AgBr]$, in their report the authors provided neither experimental nor spectroscopic details to support their claim.[16] Compounds $[PPh_4][(CF_3)_3AgBr]$ (**3**) and $[PPh_4][(CF_3)_3AgI]$ (**4**) were cleanly obtained by reaction of the fluoro complex **1** with the corresponding silyl halide Me_3SiX (Scheme 3). The isolated halide complexes $[PPh_4][(CF_3)_3AgX]$ (**1**–**4**) were increasingly colored solids along the series: F (white) < Cl (pale yellow) < Br (yellow) < I (orange).

The pseudohalide complexes $[PPh_4][(CF_3)_3AgCN]$ (**6**) and $[PPh_4][(CF_3)_3Ag(N_3)]$ (**7**) were similarly obtained by reacting the fluoro complex **1** with the appropriate Me_3SiX' reagent (X′ = CN, N_3). Following this procedure, the cyano complex **6** is obtained virtually free of contaminants, whereas it contained about 5% of the homoleptic compound $[PPh_4][(CF_3)_4Ag]$ when obtained by treatment of $[PPh_4][trans\text{-}(CF_3)_2Ag(CN)_2]$ with AcCl.[15] The azido complex **7** is particularly interesting given the relevance of the azide group in silver chemistry.[25] The binary silver(I) azide, $Ag(N_3)$, has been known for more than a century:[26] its explosive behavior has attracted much attention and has been thoroughly studied.[27] Considering the potential explosive nature of the new compound **7**, only small amounts were prepared in each synthetic batch and the solid samples were handled with great caution. Nevertheless, in our experience, compound **7** proved to be not particularly sensitive to heat and shocks. It can be described as a moderately stable compound decomposing without exploding at 92 °C (TGA: Figure S36 in the Supporting Information). This behavior can be associated to the large size of the cation, as found in several homoleptic azides of various transition metals.[28] To the best of our knowledge, no silver(III) azide had been isolated thus far. In contrast, several azides of Au^{III} are currently known, including the neutral compounds $(NHC)Au(N_3)_3$,[29] (terpy-κN)$Au(N_3)_3$,[30] and (N&C)$Au(N_3)_2$,[31] as well as the cationic complex $[(BPI)Au(N_3)][PF_6]$[32] and different salts of the homoleptic complex $[Au(N_3)_4]^-$.[28,33] The isolation of compound **7** lends support to the existence of the formally related species $[Ag(OH)_3(N_3)]^-$, which, according to kinetic and mechanistic studies, was suggested to operate as a key intermediate in the reduction of Ag^{III} by azide in aqueous alkaline media.[34]

Spectroscopic characterization

All the compounds described here have been characterized by analytical and spectroscopic methods. The results are given in the Experimental Section and the original spectra are shown in the Supporting Information. In the following discussion, especial emphasis will be put on the comparison of the data presented here with those already known for the homologous gold(III) derivatives, $[(CF_3)_3AuX]^-$, wherever such comparison can be established.[18] This will enable to evaluate from an experimental viewpoint to which extent these twofold Ag^{III} / Au^{III} series show similar properties as should be expected for isoleptic and isoelectronic species. This experimental relationship is of particular importance considering that the oxidation

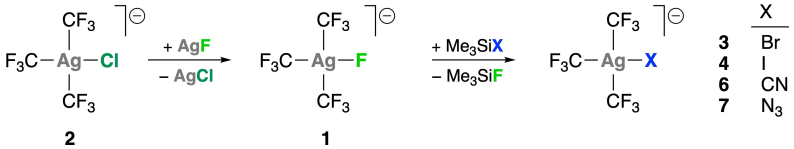

Scheme 3. Synthesis of the organosilver(III) halide and pseudohalide complexes $[(CF_3)_3AgX]^-$.

state of related Cu^{III} species has been questioned and is still much debated.[35–37]

The IR spectra are shown in Figures S1–S6. Here, only the most relevant features will be commented on. The absorption assigned to the M–Cl stretching mode in compound **2**, ν(Ag–Cl) = 348 cm^{-1} (Figure S2), appears at slightly higher frequency than observed in the corresponding gold homologue: ν(Au–Cl) = 341 cm^{-1}.[18] This is the standard trend in ν(M–X) vibrations of 4d versus 5d metals, as exemplified in the case of the Pd^{II} / Pt^{II} couple,[38] which is isoelectronic (d^8) with the Ag^{III} / Au^{III} one. The standard trend is reversed in the fluoro complexes, since the ν(M–F) vibration in compound **1** (Figure S1) appears at lower frequency (492 cm^{-1}) than that observed for gold (511 cm^{-1}).[18] Given that the metal coordination environment and even the cation are exactly the same in both cases, $[PPh_4][(CF_3)_3MF]$ (M = Ag, Au), the reverse trend observed here would suggest that in these compounds, the Ag–F bond is weaker than the Au–F one. It is worth noting that the IR-active $\nu_a(MF_4)$ stretching mode (E_u) in the simple $Cs[MF_4]$ salts appears again at higher frequency for Ag (595 cm^{-1})[39] than for Au (585 cm^{-1}).[40] In the cyano complex **6**, no absorption is observed that might be assigned to the ν(CN) vibration (Figure S5). As this vibration mode should be IR active in a local C_s symmetry (see structural data below), the failure to observe the corresponding absorptions in the $[PPh_4][(CF_3)_3MCN]$ compounds can be due to just poor intensity in both cases (M = Ag, Au). The absorption appearing at 407 cm^{-1} in compound **6** can be ascribed to the ν(Ag–CN) vibration. In the homologous gold compound, the corresponding ν(Au–CN) absorption appears at 425 cm^{-1}.[18] The azido complex **7** shows a sharp absorption at 2042 cm^{-1} (Figure S6), which can be assigned to the ν_a(NNN) mode. An additional absorption at 396 cm^{-1} can be ascribed to the ν(Ag–N) vibration mode, as typically found in terminal M–N_3 complexes.[41]

The ^{19}F NMR spectra of the $[(CF_3)_3AgX]^-$ compounds are particularly rich and informative (Figures S7–S18). They all consist of basically a quartet and a septet in 2:1 integrated ratio, corresponding to the two chemically inequivalent CF_3 groups in each molecule, namely the mutually perpendicular CF_3–Ag–CF_3 (*trans*) and CF_3–Ag–X (*trans*) units. This basic pattern undergoes further splitting by coupling to the $^{107}Ag/^{109}Ag$ nuclei with 51.84:48.16 natural abundance[42] — both of them with nuclear spin $I = {}^1/_2$. The resulting pattern can appear therefore complex in aspect. Nevertheless, the spectral parameters can be directly obtained from the experimental spectra. The accuracy of the analysis was further checked by simulation (see Supporting Information). The spectroscopic data of the cyano complex (**6**) and the heavier halides (**2**–**4**) had been masterfully assigned by Eujen and his coworkers relying on solutions samples.[15] Our data generally agree with their assignments and will not be described in detail here. In the spectrum of the fluoro-derivative **1** (Figure S7), the complex signal at high field ($\delta_F = -236.22$ ppm) is assigned to the terminal F-ligand. The resonances of the chemically inequivalent CF_3 groups show the largest separation within the halide series ($\Delta\delta \approx 13$ ppm). The separation decreases markedly in the chloro complex **2** ($\Delta\delta = 5$ ppm), becomes very small in the bromo complex **3** ($\Delta\delta \approx 0.6$ ppm) and turns inverted in the iodo complex **4** ($\Delta\delta \approx -8$ ppm). The chemical shift of each kind of CF_3 group shows almost linear dependence of the electronegativity of the involved halogen, χ(X), measured in the Sanderson scale (Figure 1).[43] The dependence is more pronounced in the mutually *trans* CF_3 groups than in the one *trans* to the varying substituent X. This surprising dependence was already observed in the homologous gold(III) system,[18] as well as in the related set of isoleptic and isoelectronic platinum(II) derivatives $[(CF_3)_3PtX]^{2-}$ (X=Cl, Br, I).[44] In the cyano complex **6**, the positions of the nominal septet versus quartet signals appear also inverted ($\Delta\delta \approx -5$ ppm), as is usually found in square-planar $[(CF_3)_3MX]^{n-}$ complexes with anionic and neutral π-acceptor ligands (e.g., CN, CO, CNR, PR_3), and also with X=I.[17,18,44]

In the ^{19}F NMR spectrum of the azido complex **7**, all fine features are clearly resolved (Figure 2). The positions of the nominal septet ($\delta_F = -25.76$) and quartet ($\delta_F = -35.02$) are near the positions observed in the fluoro complex **1** ($\delta_F = -24.43$ and -37.60 ppm, respectively). The remarkable spread of CF_3 signals observed for the $[(CF_3)_3Ag(N_3)]^-$ anion ($\Delta\delta \approx 9$ ppm) and the fluoro complex **1** ($\Delta\delta \approx 13$ ppm) denotes largely different chemical environments for the two inequivalent CF_3 groups in both anionic species.

Experimental ground-state structures

The isolation of the $[(CF_3)_3AgX]^-$ complexes **1**–**4** provides an unprecedented opportunity to obtain structural information on the Ag(III)–X bonds (X = Cl, Br, I). Single crystals were obtained for all the compounds described here and were studied by X-ray diffraction (XRD) methods. Unfortunately, the anion of the iodo complex **4** suffered from heavy disorder of the substituents around the metal, thus precluding to obtain the desired structural parameters in this case. In the previously reported κ_L-(BEDT-TTF)$_2$[$(CF_3)_3AgCl]\cdot CHCl_2CH_2Cl$ salt (monoclinic, *Pnma*),[45] the anion was also heavily disordered and thus no detailed

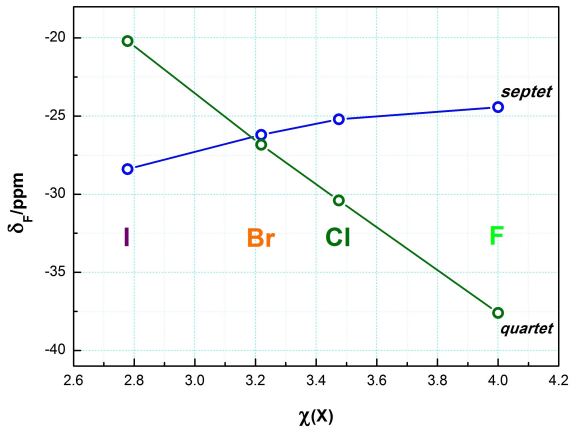

Figure 1. Correlation between the δ_F values of the $[PPh_4][(CF_3)_3AgX]$ compounds **1**–**4** (^{19}F NMR in CD_2Cl_2 solution at room temperature) and the electronegativity of the halogen involved, χ(X), on the Sanderson scale.[43]

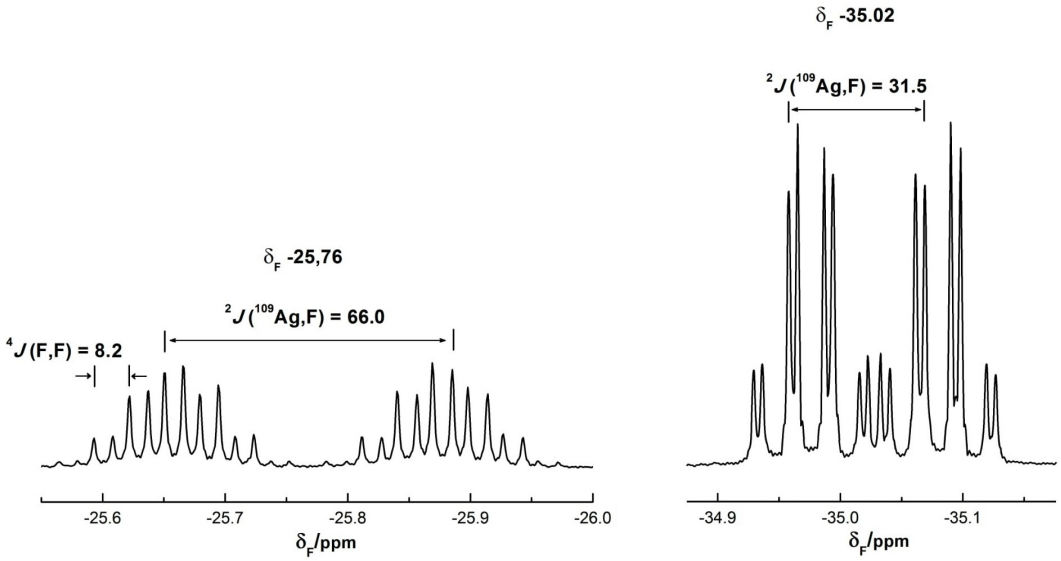

Figure 2. ^{19}F NMR spectrum of the azido complex **7** in CD_2Cl_2 solution at room temperature with relevant parameters indicated (δ_F in ppm; J in Hz). The ratio of the couplings to the ^{109}Ag and ^{107}Ag isotopes in each case is the ratio of their respective gyromagnetic constants: $\gamma(^{109}Ag)/\gamma(^{107}Ag) \approx 1.15$.

structural information could be gained, either. In turn, the diffraction experiments of compounds **1–3** were satisfactory as detailed in the Supporting Information.[46] In the obtained structures, cations and anions appear separated in the crystal lattices except for the fluoro complex **1**. In the latter case, the terminal F ligand forms loose [Ag]–F···HC(sp^2) hydrogen bonds with the cation, as already pointed out in our previous communication.[14] The experimentally obtained structures of the $[(CF_3)_3AgX]^-$ anions (X=F, Cl, Br) are invariably square-planar (Figure 3), as is usually found in d^8 metal complexes. The most relevant geometric parameters are given in Table 1, where they are compared with those corresponding to the all-organo-metallic $[PPh_4][(CF_3)_3AgR]$ compounds (R=CH_3,[15] CF_3).[19] The geometry of the CF_3–Ag–CF_3 axis shows little variation along the series, being almost linear and with Ag–C bond distances of approximately 210 pm. The Ag–C bond in the perpendicular CF_3–Ag–X axis is shorter, which is consistent with the lower *trans* influence of the halide ligands.[47] The Ag–C bond in the CF_3–Ag–F unit (**1**) is particularly short (203.6(2) pm), while the associated Ag–F bond (198.4(1) pm) is longer than that found in the purely inorganic salt $K[AgF_4]$: 188.9(3) pm.[48] The observed elongation of the Ag–F bond in compound **1** can be ascribed to the comparatively larger *trans* influence of the CF_3 group.[49] The Ag–F bond distance in compound **1** is identical to that found in the naked diatomic silver(I) fluoride molecule AgF in the gas phase: 198.32 pm.[50] This coincidence is surprising considering the different oxidation state and coordination number of the metal in each case. The observed Ag–X bond distances in compounds **2** and **3** (Ag–Cl 232.03(4) pm; Ag–Br 246.25(2) pm) are, in turn, slightly longer than those found in gaseous AgX: Ag–Cl 228.08 pm and Ag–Br 239.22 pm.[51]

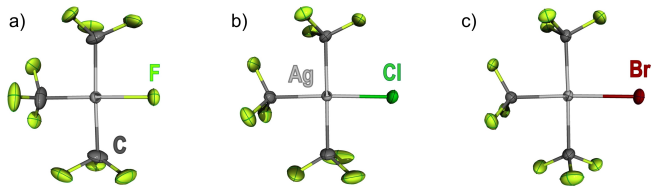

Figure 3. Displacement-ellipsoid diagram (50% probability) of the organo-silver(III) anionic complexes: a) $[(CF_3)_3AgF]^-$ in **1** (see ref. [14]), b) $[(CF_3)_3AgCl]^-$ in **2**, and c) $[(CF_3)_3AgBr]^-$ in **3**.

Table 1. Relevant structural parameters of the $[PPh_4][(CF_3)_3AgX]$ salts, as determined by single-crystal XRD methods.[a]

X	Ag–X [pm]	XAg–CF_3[b] [pm]	Ag–C_2[c] [pm]	C–Ag–X[d] [°]	$\Sigma\angle$[e] [°]
CH_3[f]	209.7(5)	212.7(5)	211.5(5)	173.8(2)	360.4(2)
CF_3[g]	209.8(2)	209.8(2)	209.8(2)	176.8(1)	360.07(9)
F (**1**)[h]	198.4(1)	203.6(2)	209.8(2)	179.46(7)	359.98(8)
Cl (**2**)	232.03(4)	206.7(2)	212.3(2)	177.87(5)	359.97(7)
Br (**3**)	246.25(2)	207.7(2)	211.2(2)	175.03(9)	359.8(1)
CN (**6**)	204.0(2)	207.1(2)	210.4(2)	178.47(7)	360.08(8)
[Au]–CN[i]	*[205.9(3)]*	*[206.8(3)]*	*[211.2(3)]*	*[178.50(9)]*	*[360.0(1)]*
N_3 (**7**)	205.6(5)	202.9(7)	210.6(13)	176.2(3)	360.0(3)

[a] Average values indicated where not unique. [b] The Ag–C distance *trans* to X is here indicated. [c] Average of the two independent Ag–C bond lengths in *trans* arrangement. [d] Nearly linear *trans*-standing C–Ag–X unit. [e] Summation of all adjacent E–Ag–E′ angles as a measure of planarity. [f] Ref. [15]. [g] Ref. [19]. [h] Ref. [14]. [i] The gold compound $[PPh_4][(CF_3)_3AuCN]$ is included here for comparison: see Ref. [18].

It would be useful to compare the structural parameters obtained for the silver(III) halide complexes **1–3** with their gold (III) homologues. These compounds are indeed known,[18] but their structures have not yet been determined by XRD methods. The desired comparison can, however, be established between the corresponding cyano complexes $[PPh_4][(CF_3)_3MCN]$ (M=Ag (**6**) and Au). This comparison is particularly reliable, since the

diffraction data of these isomorphous single crystals (monoclinic, $P2_1/c$, $Z=4$) with very similar lattice constants and virtually the same cell volume, were also taken at the same temperature (100 K) and were solved to similar final accuracy levels producing comparable standard deviations. The obtained structural parameters around the metal are virtually identical

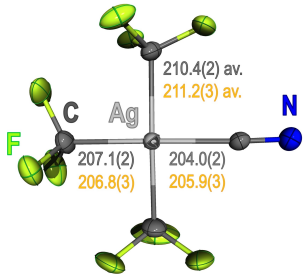

Figure 4. Displacement-ellipsoid diagram (50% probability) of the anion $[(CF_3)_3AgCN]^-$ as found in crystals of **6**.[46] The M–C bond lengths (in gray) are compared with those found in the isomorphous homologous gold compound $[PPh_4][(CF_3)_3AuCN]$ (in yellow).[18]

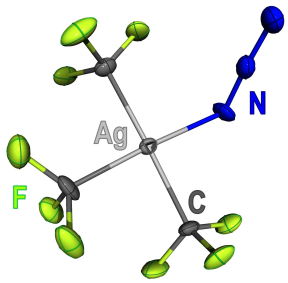

Figure 5. Displacement-ellipsoid diagram (50% probability) of the anion $[(CF_3)_3Ag(N_3)]^-$ as found in crystals of **7**.[46]

within the experimental error in both compounds (Figure 4 and Table 1) and confirm our former conclusion that Ag^{III} and Au^{III} have similar covalent radii, at least in square-planar coordination environments.[52]

The structure of the anion $[(CF_3)_3Ag(N_3)]^-$ as found in crystals of **7** is depicted in Figure 5.[46] The azide unit is almost linear: N^α–N^β–N^γ 175.0(5)°. It acts as a terminal ligand with a distinct bent arrangement, Ag–N^α–N^β 120.9(5)°, and a twist out of the metal coordination plane by 51.9(4)°. The N^α–N^β bond is slightly elongated: N^α–N^β 119.8(7) pm versus N^β–N^γ 115.4(6) pm; $\Delta r = 4.4$ pm.[53] The latter feature is characteristic of a significant degree of covalency in the M–N_3 interaction and is in keeping with the ν_a(NNN) vibration observed in the IR spectrum of **7** (see above).[53] The Ag–N distance (205.6(5) pm) is significantly shorter than found in the linear silver(I) complex (SIDipp)Ag(N_3) (209.5(2) pm)[54] and in the terminal moiety of the homoleptic silver(I) complex $[PPh_4][Ag(N_3)_2]$: 213.9(4) pm.[25]

Calculated ground-state structures

The geometries of the individual $[(CF_3)_3AgX]^-$ anions have been optimized (DFT/M06) and the results are shown in Figure S43. The obtained square-planar geometries are energy minima for every halogen, including the heaviest naturally occurring one X=At (**5**). The calculated structures of the lighter halogens (X=F, Cl, Br) show reasonable agreement with those established by XRD for compounds **1**–**3** (Figure 3). The observed differences in the corresponding Au–X bond lengths are <5 pm in every case. The electronic structures have also been systematically calculated and analyzed in order to determine some periodic trends along the halogen Group with special focus on the Ag^{III}–X bonding. The energy levels are compared in Figure 6a

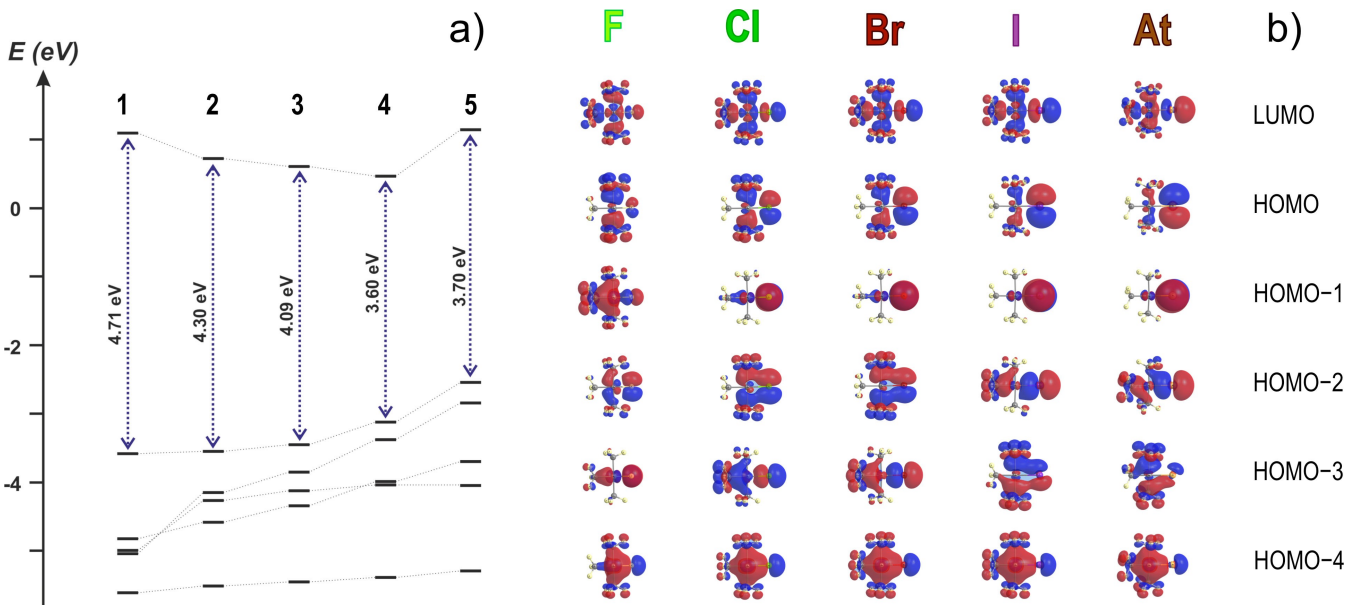

Figure 6. a) Energy levels and b) contour isosurfaces (isovalue: 0.02) of the frontier orbitals and near lower MO's of the $[(CF_3)_3AgX]^-$ complexes **1**–**5** obtained at the DFT/M06 level of theory. More complete sets including the MOs with main M(d) contribution are shown in Figures S47 and S48.

and the frontier MO contours of all these C_s complexes are shown in Figure 6b.

The HOMO–LUMO gap (Figure 6a) is largest for the fluoro complex **1** (4.71 eV) and decreases monotonically up to the iodo complex **4** (3.60 eV). The slight increase calculated for the astato complex **5** (3.70 eV) is due to destabilization of the LUMO. The LUMO and HOMO sets in the full series of complexes **1**–**5** are consistently ligand-based orbitals in all cases (Figure 6b). The a′ LUMO set is mainly antibonding with regard to the Ag–X and all the Ag–C interactions. The a′′ HOMO is, in turn, mainly bonding with regard to the *trans* C–Ag–C σ-bond system with anti-phase minor contribution of the in-plane X(p_x) orbital. This MO acquires increasing X(p) character down the Group and is particularly destabilized for the heaviest halogens I and At. The immediately lower orbitals are roughly similar for complexes **2–5** but show significant reordering in the lightest complex **1**. For this reason, we will focus on the chloro-derivative **2** as the model compound and will derive all the other therefrom.

The HOMO-1 level in complex **2** mainly involves the X(p_z) orbital with just a marginal antiphase contribution of the M(d_{yz}) orbital. This virtually nonbonding a′ MO is the HOMO-1 in complexes **2**–**5** and appears as the HOMO-3 level in complex **1**. It occurs perpendicular to the coordination plane (*xy*) and shows the largest energy variation along the series, in line with the increasing destabilization of the X(p) atomic orbitals down the halogen Group.

In the HOMO-2 level of complex **2** there is some π-bonding overlap of the anti-phase C–Ag–C (*trans*) unit with the in-plane X(p_x) orbital. There is also just a marginal contribution of the M(d_{xy}) orbital. This a′′ MO lying in the coordination plane (*xy*) appears as the HOMO-2 level in complexes **1**–**3** and as the HOMO-3 level in complexes **4** and **5**. It shows little energy variation along the series except for the fluoro complex **1**, where it appears substantially stabilized. The corresponding MO with the dual Ag–X π-antibonding interaction (a′′) is the HOMO in all cases.

The HOMO-4 level is a bonding MO (a′) encompassing the whole C_3AgX unit and involving a hybrid sd_{z^2} metal orbital as well as the in-phase X(p_y) AO. This MO is common to all compounds **1**–**5** and shows small energy variation along the series. The energy dependence is more pronounced in the corresponding a′ MO, which involves an antiphase X(p_y) contribution and is therefore antibonding with respect to the Ag–X unit. This level appears scattered through the series, as HOMO-1 (F), HOMO-3 (Cl, Br) and HOMO-2 (I, At).

It is worth noting that the metal d orbitals are just marginally involved in the frontier orbitals or the four lower levels. The (d_{xy}, d_{xz}, d_{yz}) threefold appears as HOMO-5, HOMO-6 and HOMO-7 (Figure S48). Finally, one has to dive into the HOMO-10 to find the MO with major d_{z^2} metal contribution (Figure S48) and even below to find the $d_{x^2-y^2}$ metal orbital. This non-standard arrangement of the metal d orbitals is characteristic of inverted ligand field[36] and was also identified in the related homoleptic complex $[(CF_3)_4Ag]^-$.[19]

The topological analysis of the electron density in compounds **1–5** using the quantum-theory of atoms in molecules (QTAIM)[55] gives a rather homogeneous picture, as shown in Figure S45 and Table 2. The critical point along the Ag–X bonding path (BCP) shows just a marginal shift towards the halogen ligand (in % of the corresponding bond length) with decreasing X electronegativity. Most importantly, the electron density $\rho(\mathbf{r})$ on that critical point substantially decreases down the Group indicating a decrease in the Ag–X bond strength. The positive values of the Laplacian denote strongly polar Ag–X bonds with substantial ionic character, especially for the fluoro complex **1**, where $\nabla^2\rho(\mathbf{r}) = 0.544$ au. The ionic component also decreases down the Group reaching its minimum for the heaviest halides I and At.

We conclude that compounds **1–5** are stable chemical species exhibiting inverted ligand field. The intrinsically stable Ag–X bonds show no anomalous variation with respect to the X ligand as follows from the QTAIM analyses. Now, a critical evaluation of the most plausible decomposition paths will enable us to identify the weakest flanks in the $[(CF_3)_3AgX]^-$ complexes and thereby to test the strength of the Ag–X bonds, as will be discussed next.

Stability assessment

Only the isolation of a chemical substance enables a reliable determination of its stability. The presence of solvents or any accompanying byproduct can largely alter the intrinsic decomposition routes and further open new ones. The most efficient way to avoid the involvement of any spurious mechanism is to study the evolution of a given chemical substance in the gas phase by multistage mass spectrometry (MS^n) under collision-induced dissociation (CID) conditions.[56] We have performed these measurements for all the compounds isolated in this work. The singly charged $[(CF_3)_3AgX]^-$ anions are efficiently transferred to the gas phase under mild ionization conditions (see the Experimental Section). The MS^2 results are shown in Figures S19–S24. The energy profiles of the experimentally observed decomposition paths together with other potentially reasonable mechanisms were mapped by theoretical methods (Schemes S1–S7). A selection of the most relevant processes is

Table 2. Critical-point (CP) topology of the Ag–X bond path (BP) in the $[(CF_3)_3AgX]^-$ anions.[a]

X	F	Cl	Br	I	At
$\rho(\mathbf{r})$ [au]	0.099	0.076	0.068	0.058	0.065
$\nabla^2\rho(\mathbf{r})$ [au]	0.544	0.221	0.155	0.086	0.088
ellipticity, ε	0.032	0.025	0.015	0.006	0.008
Ag–X[b] [pm]	198.4(1)	232.03(4)	246.25(2)	–	–
BP length [pm]	198.9	236.2	250.2	269.8	267.1
r_b(Ag)[c] [pm]	104.5	114.1	118.5	125.0	123.7
r_b(X)[c] [pm]	94.4	122.1	131.7	144.8	143.4
$G(\mathbf{r})$ [au]	0.151	0.071	0.053	0.035	0.040
$V(\mathbf{r})$ [au]	−0.165	−0.087	−0.067	−0.048	−0.058
$H(\mathbf{r})$ [au]	−0.015	−0.016	−0.014	−0.013	−0.018
$G(\mathbf{r})/\rho(\mathbf{r})$	1.518	0.933	0.778	0.599	0.611

[a] Contour diagrams are shown in Figure S45. [b] Experimental values from XRD analysis (Table 1). [c] The bonded radii r_b(Ag) and r_b(X) along the Ag–X axis are defined as the distance of the BCP from the given nucleus.

shown in Scheme 4 and the calculated energy values are gathered in Table 3. Since both calculation and experiment were carried out in the gas phase, the results obtained from each method are directly comparable[57] and will be discussed jointly.

Our main concern throughout the present study was to check the stability of the Ag^{III}–X bond. To our surprise, this unit proved to be remarkably stable even for the heavier halides Br and I. According to our calculations, simple halide X^- dissociation (Scheme 4, path 1) should be a highly endergonic process requiring energies in the range 74.5–50.3 kcal mol^{-1} (Table 3, entry 1). This heterolytic dissociation would render the neutral $(CF_3)_3Ag$ moiety, which would not be observable by MS^n techniques. Hence, we specifically looked for the presence of any released X^- anion as a fingerprint of this dissociation path, but none was experimentally observed.[58,59] It can therefore be concluded that heterolytic halide dissociation does not take place under the measuring conditions, in agreement with the high energy estimated for the process. Homolytic dissociation of the Ag–X bond would invariably render the homoleptic organosilver(II) ion $[(CF_3)_3Ag^{II}]^-$ (Scheme 4, path 2), which was not observed in any of our experiments. Homolytic Ag–X dissociation would require energies in the 68.4–37.3 kcal mol^{-1} range (Table 3, entry 2).[60] It must be noted, however, that the T-shaped, open-shell species $[(CF_3)_3Ag^{II}]^-$, if formed, should be unstable and would readily evolve into the known linear anion $[CF_3AgCF_3]^-$ by spontaneous (−1.2 kcal mol^{-1}) radical dissociation of the elongated stem CF_3 group (*trans* to the void), which bears 60% spin density of the unpaired electron.[35,61] Except in the case of the fluoro-derivative **1** (Figure S19), the homoleptic organosilver(I) ion $[CF_3AgCF_3]^-$ was actually observed as a minor species in every other MS^2 spectra (Figures S20–S22). This anion, however, might also arise if the stepwise radical splitting took place in reverse order, that is, $CF_3^\bullet$ followed by $X^\bullet$ dissociation (Scheme 4, paths 6 and 7). A concerted reductive elimination of X–CF_3 from the parent ion might also occur (Scheme 4, path 8). Although energetically favored, this process would entail a transition state located at $\Delta G^{\neq}$ = 41.8–31.8 kcal mol^{-1} (Table 3, entry 8). These values suggest that the concerted reductive elimination of X–CF_3 can be discarded for the fluoro complex **1**, but may become feasible for the heavier halides. In any case, the higher energy required for the process would justify the presence of the $[CF_3AgCF_3]^-$ ion as a minor product.

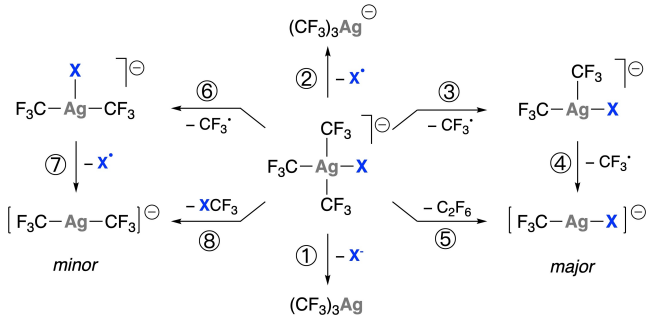

Scheme 4. Most relevant unimolecular fragmentation processes potentially operating in the $[(CF_3)_3AgX]^-$ anions. Calculated ΔG° values are given in Table 3. Unabridged mappings are given in Schemes S1–S7.

Table 3. Standard free-energy values, ΔG° [kcal mol^{-1}], calculated for the indicated dissociation processes in the $[(CF_3)_3AgX]^-$ anions.[a]

Process[b]	X=F	X=Cl	X=Br	X=I	X=At
1	74.5	57.2	54.0	50.3	49.6
2	68.4	58.3	46.0	37.3	34.1
3	24.8	19.8	19.5	18.6	19.3
4	1.1	0.1	0.3	−0.5	−0.2
5[c]	[37.9]$^{\neq}$	[33.5]$^{\neq}$	[32.3]$^{\neq}$	[31.7]$^{\neq}$	[31.8]$^{\neq}$
	−55.3	−61.3	−62.0	−63.1	−62.0
6	35.3	30.4	26.7	22.1	19.8
7	32.0	26.7	18.1	14.0	13.1
8[c]	[41.8]$^{\neq}$	[40.3]$^{\neq}$	[37.8]$^{\neq}$	[31.8]$^{\neq}$	[29.1]$^{\neq}$
	−52.4	−20.8	−16.2	−13.2	−12.7

[a] More complete sets of possible fragmentation paths are given in Schemes S1–S5. [b] Numbering as in Scheme 4. [c] The value in square brackets indicates the energy of the corresponding transition state, $\Delta G^{\neq}$ [kcal mol^{-1}].

The major species invariably observed upon fragmentation of the corresponding parent ions (Figures S19–S22) were the mixed organosilver(I) halide complexes $[CF_3AgX]^-$, where the Ag–X unit is still preserved. This entity results from the loss of a C_2F_6 mass, which may occur following a concerted or a stepwise mechanism. The former (Scheme 4, path 5) is hampered by a high-energy transition state ($\Delta G^{\neq}$ 37.9–31.7 kcal mol^{-1}). The latter (Scheme 4, paths 3 and 4) is actually the least energetically demanding of all the primary dissociation paths under study (Table 3): Homolytic splitting of the first Ag–C bond in the CF_3–Ag–CF_3 axis requires $<$25 kcal mol^{-1}, whereas the second will take place at virtually no energy cost ($\leq$ 1.1 kcal mol^{-1}).[61] Consequently, this is the suggested mechanism to account for the major signals observed in every MS^2 experiment. This fragmentation pattern is also in line with the elongated Ag–C bonds (210–212 pm) in the CF_3–Ag–CF_3 axis (Table 1). Stepwise radical dissociation of two $CF_3^\bullet$ units was also observed and demonstrated in the homoleptic organosilver(III) complex $[(CF_3)_4Ag]^-$.[35]

The geometries of the major fragmentation products $[CF_3AgX]^-$ were optimized at the DFT/M06 level of calculation. The results are shown in Figure 7. The Ag–X bond lengths in these linear molecules (d^{10}) are all very similar to those obtained for their square-planar $[(CF_3)_3AgX]^-$ counterparts (d^8). We note that the calculated Ag–Cl bond distance (235.5 pm) compares well with that experimentally established by Tyrra and Naumann in the $[N(PPh_3)_2][CF_3AgCl]$ salt: 233.88(15) pm.[62] This Ag–Cl interatomic distance is slightly longer than the Au–Cl bond length found in the homologous gold compound $[PPh_4][CF_3AuCl]$ (229.1(1) pm),[63] which is consistent with Au^I being smaller than Ag^I.[64] This difference, which has been ascribed to the particularly strong relativistic effects operating in Au^I, vanishes with the metals in the oxidation state III, as commented above.

The mixed organosilver(I) halide complexes $[CF_3AgX]^-$ were further subjected to MS^3 experiments under CID conditions (Figures S25–S28). They all undergo CF_2 extrusion eventually affording the triatomic fluoride complexes $[FAgX]^-$ [Eq. (1)], which, aside from the symmetric fluoride $[FAgF]^-$,[65] had not

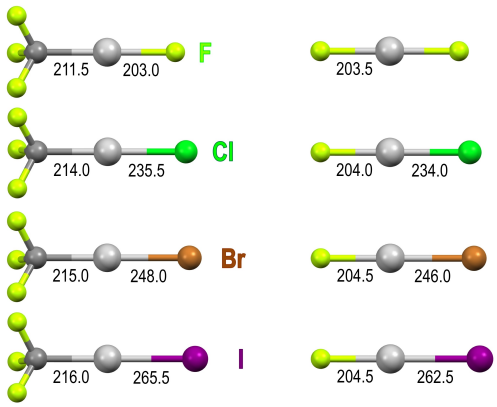

Figure 7. Optimized geometries of the anionic complexes $[CF_3AgX]^-$ (left) and the $[FAgX]^-$ (right) in the gas phase (X=F, Cl, Br, I) calculated at the DFT/M06 level. All these species were experimentally observed by multistage mass spectrometry (MS^n). Calculated Ag–C and Ag–X bond distances [pm] are indicated.

been detected thus far.[66] Given the ease with which Ag^I undergoes ligand exchange and/or associative processes in the condensed phase, these interesting silver(I) fluorohalide complexes are not likely to be isolated in pure form.

$$[F_3C{-}Ag{-}X]^{\ominus} \xrightarrow[-:CF_2]{} [F{-}Ag{-}X]^{\ominus} \quad (1)$$

The geometries of all these triatomic $[FAgX]^-$ complexes were also calculated by theoretical methods and are shown in Figure 7. The obtained interatomic distances do not substantially depart from those obtained for the parent organosilver(I) species $[CF_3AgX]^-$. The Ag–X bond distances obtained in both series of anionic complexes $[CF_3AgX]^-$ and $[FAgX]^-$ appear elongated with respect to the neutral diatomic AgX molecules (see above); this can be ascribed to the increase in both the metal coordination number and the global charge.

It is worth noting that the Ag–X bonds are preserved along the major dissociation paths in the explored MS^n experiments, thus giving proof of their intrinsic stability. In contrast, none of the initial Ag–C bonds are present in the final fragmentation products. They are broken first as the result of homolytic cleavage and then following CF_2 extrusion.

We have also studied the stability of the isolated compounds $[PPh_4][(CF_3)_3AgX]$ (**1**–**4**) in the bulk by TGA/DTA measurements (Figures S31–S34). According to the observed decomposition temperatures [°C], the stability decreases in the following order: F (145) > Cl (140) > Br (134) > I (78). We can conclude that these organosilver(III) halide complexes show remarkable stability even for the heavier halides Br and I. Nevertheless, they are less stable than the homoleptic, all-organometallic compound $[PPh_4][(CF_3)_4Ag]$, which melts at 135 °C and decomposes at 188 °C.[19] They are also considerably less stable than their corresponding gold(III) homologues $[PPh_4][(CF_3)_3AuX]$, for which the following decomposition temperatures [°C] were experimentally determined: Cl (315) > Br (295) > F (267) > I (245).[18] The large stability difference of Ag^{III} versus Au^{III} is a general feature in the chemistry of these coinage metals.

Once the decomposition temperatures were known, the thermolyses of solid samples of compounds **1**–**4** were carried out in sealed tubes (see the Experimental Section) and the soluble products formed were analyzed by ^{19}F NMR spectroscopy (Figures S37–S40). Metal deposition occurred in most cases. The homoleptic species $[(CF_3)_4Ag]^-$ invariably appears as a major decomposition product. This clearly evidences that ligand exchange takes place during the process, which marks a fundamental difference with the data obtained from our unimolecular MS^n measurements in the gas phase. Nevertheless, there is convincing evidence of $CF_3^\bullet$ radical dissociation operating also in the condensed phase. Thus, multiple, non-selective trifluoromethylation of the phenyl rings of the $[PPh_4]^+$ cation is observed together with formation of substantial amounts of CF_3H. In addition to the radical dissociation process, there is also evidence for the participation of concerted X–CF_3 elimination (Scheme 4, path 8). As already pointed out, our calculations predict an associated transition state for the latter process, the energy of which considerably decreases down the halogen Group (Table 3, entry 8). Our experimental observations nicely confirm our calculations. Thus, in the fluoro complex **1** with an associated $\Delta G^{\neq} = 41.8$ kcal mol^{-1} value, none of the required elimination products, $[CF_3AgCF_3]^-$ or CF_4, was experimentally observed in the gas phase (Figure S19) or in the condensed phase (Figure S37). By contrast, the decomposition of the iodo complex **4** produced considerable amounts of both $[CF_3AgCF_3]^-$ (Figures S22 and S40) and ICF_3 (Figure S40). This accessible decomposition path would justify the failure in the reverse reaction commented above, that is, the oxidative addition of ICF_3 onto the linear organosilver(I) derivative $[CF_3AgCF_3]^-$ (Scheme 2). Moreover, the detection of increasing amounts of X–CF_3 (Figures S37–S40) and $[CF_3AgCF_3]^-$ (Figures S19–S22) down the Group are in excellent agreement with our calculations. We conclude that the sizable energy of the transition states required to reductively eliminate CF_3–CF_3 or X–CF_3 ($\Delta G^{\neq} > 30$ kcal mol^{-1}) is a key factor determining the stability of compounds **1**–**4**.

In the solid state, the cyano complex **6** decomposes at 144 °C (Figure S35) showing therefore similar stability to the fluoro complex **1**. The azido complex **7** is, in turn, in the lower range of stability, as it decomposes at 92 °C (Figure S36). No sign of explosive or violent behavior was observed for the latter compound in the TGA/DTA experiments, in its thermolysis or in the customary laboratory handling. Even so, solid samples of **7** were always handled with caution. The bulk thermolyses of the pseudohalide complexes **6** and **7** (Figures S41 and S42) proceed in a similar way as in the halides **1**–**4**. Also the unimolecular decompositions in the gas phase are qualitatively similar, whereby the mixed species $[CF_3AgX']^-$ (Figures S23 and S24) and $[FAgX']^-$ (Figures S29 and S30) are equally observed (X′=CN, N_3). As far as we know, these species had not been previously detected with the only exception of the cyano complex $[CF_3AgCN]^-$.[15] The observed fragmentation sequence denotes that the Ag–X′ unit in compounds **6** and **7** is also surprisingly robust.

Conclusion

The isolation of the whole series of halide complexes $[(CF_3)_3AgX]^-$ (X=F, Cl, Br, I) has enabled us to establish an experimental correlation between their individual stability and the nature of the heteroligand, X. Thus, a delicate balance between radical $CF_3^\bullet$ dissociation and the reductive elimination of CF_3X is observed upon thermolysis in the gas phase that absolutely depends on the nature of X. The energy profiles for both processes have been calculated by theoretical methods. The calculated profiles for these unimolecular processes show remarkable agreement with the experimental data in the gas phase. In the solid state, however, additional intermolecular rearrangements that involve CF_3 transfer between silver centers operate. We further demonstrate that the Ag^{III}–Br and Ag^{III}–I bonds are not intrinsically unstable. The remarkable stability of our system is further effected by the sizable energy barriers associated with reductive elimination processes. In contrast, the instability of the simple AgX_3 and $[AgX_4]^-$ species with $X \neq F$ can be attributed to the ease with which X_2 is reductively eliminated. This holds true even for the binary fluoride AgF_3, which readily and spontaneously undergoes reduction in the condensed phase.[7] It should be emphasized that, in our system, inner-sphere full electron transfer from the heavier halide ligands X to the Ag^{III} center does not take place as readily as might be anticipated.

Our results prove that organosilver(III) halides are indeed feasible for every halogen, including the more polarizable and less electronegative Br and I. The implications of the stability of Ag^{III} towards halogens are substantial, particularly in the plethora of silver-mediated chemical processes as well as in fundamental chemistry. Needless to say, however, that the precise stability of any particular entity will heavily depend on the nature of the accompanying ligands at the Ag^{III} center.

Acknowledgements

This work was supported by the Spanish MICIU/FEDER (projects PGC2018-094749-B–I00 and PGC2018-093451-B–I00) and the Gobierno de Aragón (Grupo E17 20R). BIFI (Instituto de Biocomputación y Física de Sistemas Complejos) and CESGA (Centro de Supercomputación de Galicia) are acknowledged for the allocation of computational resources. D.J.-S. also thanks the Spanish MICIU for a grant (BES-2016-078732).

Conflict of Interest

The authors declare no conflict of interest.

Keywords: highest oxidation states · inverted ligand fields · organosilver · silver(III) · unimolecular processes

[1] a) L. Capdevila, E. Andris, A. Briš, M. Tarrés, S. Roldán-Gómez, J. Roithová, X. Ribas, *ACS Catal.* **2018**, *8*, 10430; b) M. Font, F. Acuña-Parés, T. Parella, J. Serra, J. M. Luis, J. Lloret-Fillol, M. Costas, X. Ribas, *Nat. Commun.* **2014**, *5*, 4373.
[2] T. Elkoush, C. L. Mak, D. W. Paley, M. G. Campbell, *ACS Catal.* **2020**, *10*, 4820.
[3] M. Malischewski, in *Comprehensive Organometallic Chemistry IV, Vol. 1* (Ed.: P. L. Holland), Elsevier, **2021**; DOI: 10.1016/B978-0-12-820206-7.00004-4.
[4] a) M. Deuker, Y. Yang, R. A. J. O'Hair, K. Koszinowski, *Organometallics* **2021**, *40*, 2354; b) S. Weske, R. A. Hardin, T. Auth, R. A. J. O'Hair, K. Koszinowski, C. A. Ogle, *Chem. Commun.* **2018**, *54*, 5086.
[5] a) A. Higelin, S. Riedel in *Modern Synthesis Processes and Reactivity of Fluorinated Compounds, Vol. 3* (Eds.: H. Groult, F. Leroux, A. Tressaud), Elsevier, Amsterdam, **2017**, Ch. 19, pp. 561–586; b) S. Riedel in *Comprehensive Inorganic Chemistry II* (Eds.: E. V. Antipov, A. M. Abakumov, A. V. Shevelkov), Elsevier, Amsterdam, **2013**, Ch. 2.08, pp. 187–221; c) S. Riedel, M. Kaupp, *Coord. Chem. Rev.* **2009**, *253*, 606.
[6] Previous reports on silver in higher oxidation states would need confirmation: a) A. I. Popov, Y. M. Kiselev, *Russ. J. Inorg. Chem.* **1988**, *33*, 541; *Zh. Neorg. Khim.* **1988**, *33*, 965; b) A. I. Popov, Y. M. Kiselev, V. F. Sukhoverkhov, V. I. Spitsyn, *Dokl. Chem.* **1988**, *296*, 424; *Dokl. Akad. Nauk SSSR* **1987**, *296*, 615; c) R. Hoppe, *Isr. J. Chem.* **1978**, *17*, 48; d) P. Sorbe, J. Grannec, J. Portier, P. Hagenmuller, *J. Fluorine Chem.* **1978**, *11*, 243; e) J. Grannec, P. Sorbe, J. Portier, P. Hagenmuller, *C. R. Acad. Sci., Ser. C* **1977**, *284*, 231.
[7] a) G. M. Lucier, J. M. Whalen, N. Bartlett, *J. Fluorine Chem.* **1998**, *89*, 101; b) B. Žemva, K. Lutar, A. Jesih, W. J. Casteel, Jr., A. P. Wilkinson, D. E. Cox, R. B. von Dreele, H. Borrmann, N. Bartlett, *J. Am. Chem. Soc.* **1991**, *113*, 4192.
[8] R. Hoffmann, *Am. Sci.* **2001**, *89*, 311.
[9] a) T. Jia, X. Zhang, T. Liu, F. Fan, Z. Zeng, X. G. Li, D. I. Khomskii, H. Wu, *Phys. Rev. B* **2014**, *89*, 245117; b) R. Hoppe, R. Homann, *Naturwissenschaften* **1966**, *53*, 501.
[10] W. Grochala, R. Hoffmann, *Angew. Chem. Int. Ed.* **2001**, *40*, 2742; *Angew. Chem.* **2001**, *113*, 2816.
[11] H.-C. Müller-Rösing, A. Schulz, M. Hargittai, *J. Am. Chem. Soc.* **2005**, *127*, 8133.
[12] M. Derzsi, A. Grzelak, P. Kondratiuk, K. Tokár, W. Grochala, *Crystals* **2019**, *9*, 423.
[13] D. F. C. Morris, *J. Phys. Chem. Solids* **1958**, *7*, 214.
[14] D. Joven-Sancho, M. Baya, A. Martín, J. Orduna, B. Menjón, *Chem. Eur. J.* **2020**, *26*, 4471.
[15] R. Eujen, B. Hoge, D. J. Brauer, *Inorg. Chem.* **1997**, *36*, 1464.
[16] D. Naumann, W. Tyrra, F. Trinius, W. Wessel, T. Roy, *J. Fluorine Chem.* **2000**, *101*, 131.
[17] A. Pérez-Bitrián, M. Baya, J. M. Casas, L. R. Falvello, A. Martín, B. Menjón, *Chem. Eur. J.* **2017**, *23*, 14918.
[18] A. Pérez-Bitrián, S. Martínez-Salvador, M. Baya, J. M. Casas, A. Martín, B. Menjón, J. Orduna, *Chem. Eur. J.* **2017**, *23*, 6919.
[19] D. Joven-Sancho, M. Baya, A. Martín, B. Menjón, *Chem. Eur. J.* **2018**, *24*, 13098.
[20] W. Dukat, D. Naumann, *Rev. Chim. Miner.* **1986**, *23*, 589.
[21] G. Helgesson, S. Jagner, *J. Chem. Soc. Dalton Trans.* **1988**, 2117.
[22] S. Ahrland, J. Chatt, N. R. Davies, *Q. Rev. Chem. Soc.* **1958**, *12*, 265.
[23] R. G. Pearson, *Chemical Hardness: Applications from Molecules to Solids*, Wiley-VCH, Weinheim, **1997**.
[24] R. J. Puddephatt, *The Chemistry of Gold*, Elsevier, Amsterdam, **1978**, Ch. 1, p. 22.
[25] T. M. Klapötke, B. Krumm, M. Scherr, *J. Am. Chem. Soc.* **2009**, *131*, 72.
[26] T. Curtius, *Ber. Dtsch. Chem. Ges.* **1890**, *23*, 3023.
[27] R. Matyáš, J. Pachman, *Primary Explosives*, Springer, Heidelberg, **2013**, Sect. 4.4, pp. 89–96.
[28] W. Beck, W. P. Fehlhammer, P. Pöllmann, E. Schuierer, K. Feldl, *Chem. Ber.* **1967**, *100*, 2335.
[29] E. Schuh, S. Werner, D. Otte, U. Monkowius, F. Mohr, *Organometallics* **2016**, *35*, 3448; NHC = 3,4-dichloro-2,5-dimethylimidazolylidene, 2,5-bis(2,6-dimethylphenyl)imidazolylidene.
[30] K. Peng, A. Friedrich, U. Schatzschneider, *Chem. Commun.* **2019**, *55*, 8142.
[31] V. Levchenko, S. Øien-Ødegaard, D. Wragg, M. Tilset, *Acta Crystallogr. Sect. E Crystallogr. Commun.* **2020**, *76*, 1725; N&C = 2-(5-ethoxycarbonylpyridin-2-yl)-5-ethoxycarbonylphenyl-κ^2C^1,*N*.
[32] T. Roth, H. Wadepohl, L. H. Gade, *Eur. J. Inorg. Chem.* **2016**, 1184; BPI = *N*,*N*′-bis(5-methylpyridin-2-yl)-1*H*-isoindole-1,3(2*H*)-diimine.
[33] a) S. Afyon, P. Höhn, M. Armbrüster, A. Baranov, F. R. Wagner, M. Somer, R. Kniep, *Z. Anorg. Allg. Chem.* **2006**, *632*, 1671; b) T. M. Klapötke, B.

Krumm, J. C. Gálvez-Ruiz, H. Nöth, *Inorg. Chem.* **2005**, *44*, 9625; c) W. Beck, T. M. Klapötke, P. Klüfers, G. Kramer, C. M. Rienäcker, *Z. Anorg. Allg. Chem.* **2001**, *627*, 1669; d) W. Beck, H. Nöth, *Chem. Ber.* **1984**, *117*, 419; e) W. Beck, W. P. Fehlhammer, P. Pöllmann, E. Schuierer, K. Feldl, *Chem. Ber.* **1967**, *100*, 2335.

[34] E. T. Borish, L. J. Kirschenbaum, *Inorg. Chem.* **1984**, *23*, 2355.

[35] M. Baya, D. Joven-Sancho, P. J. Alonso, J. Orduna, B. Menjón, *Angew. Chem. Int. Ed.* **2019**, *58*, 9954; *Angew. Chem.* **2019**, *131* 10059.

[36] R. Hoffmann, S. Alvarez, C. Mealli, A. Falceto, T. J. Cahill, III, T. Zeng, G. Manca, *Chem. Rev.* **2016**, *116*, 8173.

[37] a) I. M. DiMucci, J. T. Lukens, S. Chatterjee, K. M. Carsch, C. J. Titus, S. J. Lee, D. Nordlund, T. A. Betley, S. N. MacMillan, K. M. Lancaster, *J. Am. Chem. Soc.* **2019**, *141*, 18508; b) C. Gao, G. Macetti, J. Overgaard, *Inorg. Chem.* **2019**, *58*, 2133; c) R. C. Walroth, J. T. Lukens, S. N. MacMillan, K. D. Finkelstein, K. M. Lancaster, *J. Am. Chem. Soc.* **2016**, *138*, 1922; d) A. M. Romine, N. Nebra, A. I. Konovalov, E. Martin, J. Benet-Buchholz, V. V. Grushin, *Angew. Chem. Int. Ed.* **2015**, *54*, 2745; *Angew. Chem.* **2015**, *127*, 2783; e) G. Aullón, S. Alvarez, *Theor. Chem. Acc.* **2009**, *123*, 67; f) J. P. Snyder, *Angew. Chem. Int. Ed. Engl.* **1995**, *34*, 986; *Angew. Chem.* **1995**, *107*, 1076; g) M. Kaupp, H. G. von Schnering, *Angew. Chem. Int. Ed. Engl.* **1995**, *34*, 986; *Angew. Chem.* **1995**, *107*, 1076; h) J. P. Snyder, *Angew. Chem. Int. Ed. Engl.* **1995**, *34*, 80; *Angew. Chem.* **1995**, *107*, 112; i) D. Naumann, T. Roy, K.-F. Tebbe, W. Crump, *Angew. Chem. Int. Ed. Engl.* **1993**, *32*, 1482; *Angew. Chem.* **1993**, *105*, 1555; j) M. A. Willert-Porada, D. J. Burton, N. C. Baenziger, *J. Chem. Soc. Chem. Commun.* **1989**, 1633.

[38] F. R. Hartley, *The Chemistry of Platinum and Palladium*; Applied Science Pub., London, **1973**, pp. 240–244.

[39] A. I. Popov, Y. M. Kiselev, V. F. Sukhoverkhov, V. I. Spitsyn, *Dokl. Chem.* **1988**, *296*, 424; *Dokl. Akad. Nauk SSSR* **1987**, *296*, 615.

[40] M. A. Ellwanger, S. Steinhauer, P. Golz, H. Beckers, A. Wiesner, B. Braun-Cula, T. Braun, S. Riedel, *Chem. Eur. J.* **2017**, *23*, 13501.

[41] K. Nakamoto, *Infrared and Raman Spectra of Inorganic and Coordination Compounds. Part B*, 6th ed. Wiley, Hoboken, **2009**, pp. 129–131.

[42] J. Meija, T. B. Coplen, M. Berglund, W. A. Brand, P. de Bièvre, M. Gröning, N. E. Holden, J. Irrgeher, R. D. Loss, T. Walczyk, T. Prohaska, *Pure Appl. Chem.* **2016**, *88*, 293.

[43] a) J. E. Huheey, E. A. Kreiter, R. L. Kreiter, *Inorganic Chemistry*, 4th ed., Harper–Collins: New York, **1993**, pp. 182–199; b) R. T. Sanderson, *Simple Inorganic Substances*, Krieger Pub.: Malabar, **1989**, pp. 20–28.

[44] S. Martínez-Salvador, J. Forniés, A. Martín, B. Menjón, I. Usón, *Chem. Eur. J.* **2013**, *19*, 324.

[45] J. A. Schlueter, U. Geiser, A. M. Kini, H. H. Wang, J. M. Williams, D. Naumann, T. Roy, B. Hoge, R. Eujen, *Coord. Chem. Rev.* **1999**, *190–192*, 781; BEDT-TTF = bis(ethylenedithio)tetrathiafulvalene.

[46] Deposition Numbers 2084740 (for **2**), 2084741 (for **3**), 2084742 (for **5**), 2084743 (for **7**) contain the supplementary crystallographic data for this paper. These data are provided free of charge by the joint Cambridge Crystallographic Data Centre and Fachinformationszentrum Karlsruhe Access Structures service. See the Supporting Information for details.

[47] T. G. Appleton, H. C. Clark, L. E. Manzer, *Coord. Chem. Rev.* **1973**, *10*, 335.

[48] K. Lutar, S. Milićev, B. Žemva, B. G. Müller, B. Bachmann, R. Hoppe, *Eur. J. Solid State Inorg. Chem.* **1991**, *28*, 1335.

[49] a) A. G. Algarra, V. V. Grushin, S. A. Macgregor, *Organometallics* **2012**, *31*, 1467; b) P. Sgarbossa, A. Scarso, G. Strukul, R. A. Michelin, *Organometallics* **2012**, *31*, 1257.

[50] J. Hoeft, F. J. Lovas, E. Tiemann, T. Törring, *Z. Naturforsch., Teil A* **1970**, *25*, 35.

[51] a) L. C. Krisher, W. G. Norris, *J. Chem. Phys.* **1966**, *44*, 391; b) L. C. Krisher, W. G. Norris, *J. Chem. Phys.* **1966**, *44*, 974.

[52] A. Pérez-Bitrián, M. Baya, J. M. Casas, A. Martín, B. Menjón, J. Orduna, *Angew. Chem. Int. Ed.* **2018**, *57*, 6517; *Angew. Chem.* **2018**, *130*, 6627.

[53] By applying the correlation between structural and vibrational data recently suggested for covalent azides: $\nu_a(NNN) = 1997(4) + 11.7(4)\cdot\Delta r$ [pm] to compound **7**, the resulting value (2048 cm^{-1} for $\Delta r = 4.4$ pm) is in reasonable agreement with that experimentally observed (2042 cm^{-1}): M. Rozenberg, F. Tibika-Apfelbaum, *J. Mol. Struct.* **2013**, *1035*, 267.

[54] D. V. Partyka, T. J. Robilotto, J. B. Updegraff, III, M. Zeller, A. D. Hunter, T. G. Gray, *Organometallics* **2009**, *28*, 795; SIDipp = 2,5-bis(2,6-diisopropylphenyl)-3,4-dihydroimidazolylidene.

[55] *The Quantum Theory of Atoms in Molecules* (Eds.: C. F. Matta, R. J. Boyd), Wiley-VCH, Weinheim, **2007**.

[56] R. A. J. O'Hair, *Chem. Commun.* **2006**, 1469.

[57] J. Roithová, D. Schröder, *Coord. Chem. Rev.* **2009**, *253*, 666.

[58] Given that the MS^2 low-mass cut-off of ion-trap analyzers prevents the detection of the lighter X^- anions (see ref. [59]), the MS^2 experiments were also performed using a Q-TOF instrument (see Experimental).

[59] R. E. March, J. F. J. Tod: *Quadrupole Ion Trap Mass Spectrometry*, 2nd ed., Wiley, Hoboken, **2005**.

[60] One of the Reviewers pointed out that recombination of the $X^\bullet$ radicals into X_2 molecules would be possible in the condensed phase and would result in large stabilization of the overall system: 2 $[(CF_3)_3Ag^{III}X]^- \rightarrow 2\,[(CF_3)_3Ag^{II}]^- + X_2$. We found, however, no experimental evidence for this attractive thermodynamic channel.

[61] The spin transfer from the Ag^{II} center (d^9) to the coordinated ligands has been identified as a key source of instability: W. Grochala, Z. Mazej, *Philos. Trans. R. Soc. London Ser. A* **2015**, *373*, 20140179.

[62] a) W. Tyrra, D. Naumann, *J. Fluorine Chem.* **2004**, *125*, 823; b) W. E. Tyrra, *J. Fluorine Chem.* **2001**, *112*, 149.

[63] M. Baya, A. Pérez-Bitrián, S. Martínez-Salvador, A. Martín, J. M. Casas, B. Menjón, J. Orduna, *Chem. Eur. J.* **2018**, *24*, 1514.

[64] a) U. M. Tripathi, A. Bauer, H. Schmidbaur, *J. Chem. Soc. Dalton Trans.* **1997**, 2865; b) A. Bayler, A. Schier, G. A. Bowmaker, H. Schmidbaur, *J. Am. Chem. Soc.* **1996**, *118*, 7006; c) M. S. Liao, W. H. E. Schwarz, *Acta Crystallogr. Sect. B Struct. Sci.* **1994**, *50*, 9.

[65] N. J. Rijs, R. A. J. O'Hair, *Dalton Trans.* **2012**, *41*, 3395.

[66] A similar behavior was experimentally observed in the homologous gold system $[CF_3AuX]^-$ (X=Cl, Br, I): M. Baya, A. Pérez-Bitrián, S. Martínez-Salvador, J. M. Casas, B. Menjón, J. Orduna, *Chem. Eur. J.* **2017**, *23*, 1512.

Manuscript received: May 26, 2021
Accepted manuscript online: June 30, 2021
Version of record online: August 6, 2021